GEM TN-93-306

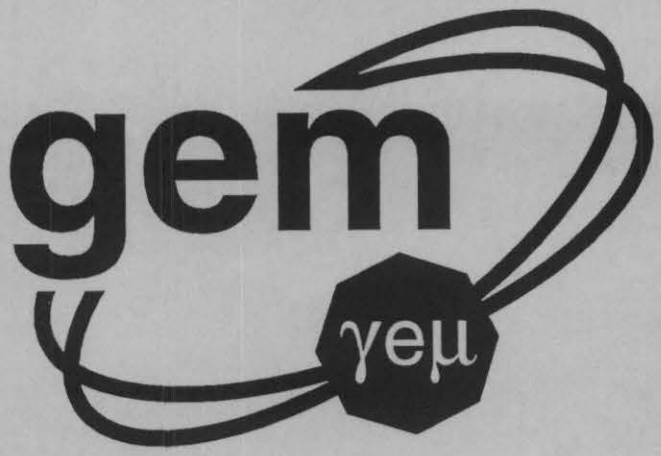

Module of Electromagnetic Secondary Emission Flight Type Calorimeter

G. S. Bitsadze[1], M. I. Chernetsov[1], Yu. V. Khrenov[2], M. Kobayashi[3], I. V. Manuilov[1], A. M. Medvedkov[1], V. I. Rykalin[1], V. T. Tolmachev[2], G. V. Zholobov[1]

[1] Institute for Higher Energy Physics, Protvino, Russia
[2] Joint Institute of Nuclear Research, Dubna
[3] KEK Tsukuba-Shi, Japan

February 1993

Abstract:

The prototype of the module of Electromagnetic Secondary Emission Flight Type Calorimeter (SEFCAL) is described. The design of the SEFCAL, first experimental results, obtained in particle beams and Monte-Carlo calculations, are presented. The energy resolution of the calorimeter for 26 GeV electrons is $\sigma_E/E=\approx 23\%$.

Module of Electromagnetic Secondary Emission Flight Type Calorimeter

G.S.Bitsadze[1)], M.I.Chernetsov[1)], Yu.V.Khrenov[2)], M.Kobayashi[3)], I.V.Manuilov[1)],A.M.Medvedkov[1)], V.I.Rykalin[1)], V.T.Tolmachev[2)], G.V.Zholobov[1)]

Abstract

The prototype of the module of Electromagnetic Secondary Emission Flight Type Calorimeter (SEFCAL) is discribed. The design of the SEFCAL, first experimental results, obtained in particle beams and Monte-Carlo calculations, are presented. The energy resolution of the calorimeter for 26 GeV electrons is $\sigma_E/E \approx 23\%$.

In known physical projects for colliders [1] the requirements to the characteristics of forward calorimeters are rather close (see Table 1). As a rule, this is a hadron calorimeter with low energy resolution, but having a radiation hardness exceeding 100 Mrad/year. Presently a new approaches to build such calorimeters are being searched for, or new types of detectors are being tested. The characteristics of the radiation hardness of some types of calorimeters-candidates are presented in Table 2.

Ionization calorimeters can be really used as forward calorimeters after resolution the problem of front-end electronic withdrawal from the detector without essential distortion of general characteristics [2].

In the last years heavy monocrystals (CeF_3, GSO) have been synthesized, which transparency changes at the level of 1% under the total doses of 100 Mrad [3] (γ

[1]Institute for High Energy Physics, Protvino, Russia.
[2]Joint Institute of Nuclear Research, Dubna.
[3]KEK Tsukuba-Shi, Japan.

source ^{60}Co). However, observed percent variation of the transparency per one radaiation length X_0 corresponds to some tens of percents for full-scale electromagnetic calorimeter of $(20 \div 25)X_0$ or hadron calorimeter with real longitudinal segmentation ($5 \div 10$ sections). Apart from this, the question of creation of the photomultiplier (PM), having the radiation hardness of tens and hundreds of Mrad is not solved yet. One also should take into account the cost of such monocrystals. For example, photon calorimeters based on GSO monocrystals with thickness of 20 X_0, would cost at least 5×10^6 US \$/m^2, according to our estimations.

A priori, secondary emission of metals and semiconductors should be little affected by radiation. Calculations of the radiation dose, absorbed by the surfaces of strong-current PM dynodes from the flux of secondary electrons during their guaranteed life-time, gives the value, which exceeds by many orders of magnitude the required one. Therefore utilization of the secondary emission for obtaining signals from shower particles in calorimeters naturally attracts the detector developers [4,5]. To verify the assumption of a potentially high radiation hardness of the secondary emission emitters, authors of the present article have measured the radiation hardness of the dynode system of the PM-110 CuAlMg-alloy dynodes. Before the PMs exposure to γ quanta from ^{60}Co, the photocurrent in the photocathode circuit and amplitudes of the output signals from the PMs to be exposed and test samples were measured. After the exposure the values of the photocathode currents and amplitudes of the signals from PMs were measured again. With integral radiation dose per week of 100 Mrad, the photocurrent of the PM-110 reduced by factor of two, which could be due to a noticeable darkening of the photocathode window. The amplification of the PMs, which is easily determined from the consideration of the photocurrent variation, changed (increased) by 5%, with a comparable measurment accuracy.

The application of microchannel plates (MCP) in sampling-calorimeters [4] actually solves the problem, with an accuracy of contradictory data about the radiation hardness of MCP and the possibility of practical implementation of such a detector.

For detection of the electromagnetic and hadronic showers the authors of the paper [5] proposed to use the secondary emission electrons, knocked out by the shower particles from the surfaces of the absorber layers. Those electrons are transported through the stacks of absorbers and amplified further by the secondary electron multiplier. The possibility of implementation such a detector was tested with the help of a three-layer prototype, irradiated by electrons, which were obtained with the help of a special emitter.

In this article the prototype of the module of electromagnetic secondary emission

flight type calorimeter (SEFCAL) is described. The Monte Carlo calculations and the first experimental results of the module study in particle beams are presented. The authors consider the development of the module as a first step on the way of hadron calorimeter creation, though the electromagnetic SEFCAL design represents an independent interest.

1. Calorimeter Module Design.

The module of the electromagnetic calorimeter is presented in fig.1. It consists of 50 layers of the absorber. Each absorber layer is a set of 100x6x1.5 mm^3 lead plates fixed on a brass frame at an angle of 45°. The front wall of each layer of the absorber has a 0.5x0.5 mm^2 small-grain metal grid to shield the surfaces of the lead plates from interlayer electric field. The absorber layers are fixed with the help of 4 glass rods and bushings (see fig.1). The distance between the layers is 2 mm. The equal potential difference is applied to the neighbouring layers of the absorber with the help of a uniform divider having a base resistance of 3 MOhm. The design of the module is actually similar to that of shutter-type dynode systems, e. g. of PM-110.

With the chosen thickness of the lead strips of 1.5 mm, the total downstream length of the module is$\approx 18X_0$, ($X_0 \approx 25$ mm is a radiation length). From the begining the number of layers was determined by the following considerations. It is known, that the secondary emission efficiency of a metal surface passed by relativistic charged particles is $2 \div 4\%$ [6] per one surface for perpendicularly incident particles. Therefore, in order to obtain a few secondary electrons from a single charged particle (muon, hadron) passing through all layers, the number of the layers should be equal to at least 50 (100 surfaces). The results of the calculations, presented below shows, that the choice of the optimal number of layers is a many-parameter problem.

The front part of the module incorporates a system of two shutter dynodes from the PM-110, one being the photo emitter and another one the cascade of secondary emission multiplication. When this system is illuminated by 10-nsec light pulses from an ultraviolet laser, the clusters of secondary electrons come on the first layer of the module. They are used as standard charged signals during capacity for work checking and the module calibration.

The back edge of the module has a secondary electron multiplier (SEM), which is a PM-49B with removed photocathode window.

2. Vacuum System.

The calorimeter module was placed into a stainless steel container of cylindrical shape having 320 mm in diameter and 900 mm long. In front part of the container there is a quartz glass window to inject a laser ray.

When manufacturing the vacuum system and module prototype, we took into account the known fact, that secondary emission multipliers are working well at the pressures below 10^{-5} torr. The required dynamic vacuum was produced by a system of forevacuum and oil-vapour pumps without outgassing of the vacuum chamber and module. In the vacuum system an oil-vapour pump AVP-05, having an air pumping rate of at least 200 l/sec, was used. The container was connected to the high-vacuum block by a tube of 100 mm in diameter and 200 mm long. A forevacuum pump 2NVR-52DM was used as an additional unit. It should be noted, that the laser signals at the SEM output appeared when a vacuum of $\leq 10^{-4}$ torr was attained, in $40 \div 60$ minutes after the beginning of pumping. During the experimental study the operational pressure of $(2 \div 4) \times 10^{-6}$ torr was attainable in $2 \div 3$ hours.

3. Measurement of the Layer Multiplication Coefficient.

One of the basic parameter of this calorimeter is a coefficient of secondary electron multiplication on the absorber layers. It should be noted, that this coefficient must be the same for all layers and close to unity, because otherwise the statistical weight of the signals coming from different layer will be different, what leads to the deterioration of the resolution. The coefficient was measured for an assembly consisting of 5 layers (see fig.3). The photocathode–secondary emitter system, similar to the one shown in fig.1, was installed in the front part of the assembly. It was illuminated by a static ultraviolet lamp. The obtained photocurrent I_0 was collected by the copper plate anode, placed immediately after it (the position is shown by the dashed line in fig.3). Then the anode was placed after 5 layers and the current I_5 was measured. The coefficient of layer multiplication k_{mult} was found from the ratio of I_0 and I_5. The measured k_{mult} dependence upon the intercascade voltage U_c is shown in fig.4. It is seen, that for the given design and material of the layer, the multiplication coefficient k_{mult} varies from 0.85 to 1.2.

4. Study of the Secondary Emission Flight Type Calorimeter Module Characteristics.

The characteristics of the calorimeter module were studied with the help of an ultraviolet laser and in particle beams.

Excitation of the calorimeter module by a pulsed laser (see fig.2) allows one to make a routine control of its workability and what is more important, to determine the nature of signal fluctuations and the linearity of the whole system versus the value of charge of secondary electrons clusters, injected into the module. The clusters charge was varied by the laser beam attenuation by plexiglas plates. The relative value of the laser light pulses was measured independently with the help of a sun blind vacuum photoelement, detecting reflected light from the optical input window. For illustration, fig.5 shows the amplitude spectra of signals at the module output, corresponding to unattenuated laser ray (the right-hand spectrum) and laser ray, passing through the plexiglas plate of 18 mm (the left-hand spectrum). Figure 6 presents the $(2\tau/\mathrm{A})^2$ dependence upon 1/A, where 2τ is FWHM, A is the mean amplitude of the module signals amplitude spectrum. The dependence is linear and crosses 0, pointing to the linearity of the detecting system (including the electronics) and to the Gaussian nature of fluctuations, which is related only with the mean number N_e of secondary emission electrons at the SEM input. Indeed, for Gaussian distribution $2\tau \sim \sqrt{N_e}$, and from the linearity $N_e \sim$A.

The characteristics of the calorimeter, exposed to particles, were studied in 26 GeV/c electron and muon beams. The momentum beam spread was $\Delta p/p \approx 1\%$. The output signals from the calorimeter module were sent to 12-bit ADC[7] . The amplitude spectra for 26 GeV electrons, measured for various values of the inter-cascade voltage U_c, are shown in fig.7 a,b,c,d. From comparison of the spectra it is seen, that with an increase of U_c, which corresponds to a growth of the multiplication coefficient k_{mult}, the resolution deteriorates. The best resolution of the calorimeter module, obtained at k_{mult}=1.15 for 26 GeV electrons, is $\sigma_E/E \approx 23\%$.

Figure 8 shows the amplitude spectrum for muon passing through all calorimeter layers. The efficiency of the muon detection is about 50%.

5. Monte Carlo Simulation. Comparison with the Experiment

The detailed simulation of the physical processes, determining the physical result under study, simplifies essentially the search for the optimal parameters and operational modes of the calorimeter. The model we used is described in brief below.

The electromagnetic shower for the specified geometry of the calorimeter was simulated with the help of the GEANT code [8]. The development of the shower was traced up to the minimum kinetic energy realized in the code, 10 KeV. During the simulation of secondary emission electrons it was assumed, that every particle of the shower, when crossing the absorber surface, knocks out of it a slow secondary emission electron with a probability of w≈(2÷4)% [6]. During the transportation of secondary emission electrons by electric field to the anode, they undergo collisions with the absorber plates. In each collision the number of electrons is varying in accordance with the Poisson law and is determined by the layer multiplication coefficient k_{mult}. Its value is close to unity and, as it was shown above, depends on the intercascade voltage. Hence, the model under consideration depends on two parameters, k_{mult} and w. The simulation results are presented in Table 3. In the computations the angular dependence of w was not taken into account and its value for perpendicularly incident particles was used. Besides, the exact value of w is not known for the lead surface having a natural oxide film, which should increase w, similarly to the CsI film influence [9]. Hence, the results mainly allow one to trace the dependence of the energy resolution and other characteristics of the detector from various parameters.

The results presented in Table 3 were obtained at energies of 5 and 26 GeV (column 2), for various values of the geometric parameters of the module: the thickness of the absorber plates (column 4) and their transverse dimensions (column 9). The dependences of the detector characteristics on the parameters w (column 3) and k_{mult} (column 10) were studied. In the case of the calorimeter depth segmentation, we indicate the segmentation structure (the number of layers in each section) by small prints in coloumn 5. The set of arrows under the digits indicates the directions of secondary emission electrons collection in sections. The standard for nonsegmentation case downstream direction is not specified. Columns 6÷8 present the energy resolution σ_E/E recalculated to 1 GeV, the number of secondary emission electrons N_e and the energy deposition ΔE in the calorimeter, respectively. At the points of Poisson fluctuations absence, the calorimeter structure is the same, as

in the previous points.

Some results calculated for 5 and 26 GeV are presented in figs.9÷11, respectively. Figure 9 shows the spectrum of the total energy deposition in the calorimeter (in % of the particle energy causing the shower), the longitudinal and transverse distributions of the shower and the measured charged spectrum (distribution N_e), in the absence of the Poisson fluctuations of secondary emission electrons number. Figures 10÷11 show the charged longitudinal shower profile and the charged spectra for different values of the parameters w and k_{mult} at 5 and 26 GeV. The global title in figs.9÷11 characterizes the energy, the thickness of the plates, the number of layers and the transverse module dimensions in cm^2.

Before going over the discussion of the data of Table 3, let us make the following two remarks:

1. To check an accuracy level of the simulation code we have done calculations for a 4x4 cm^2 cell of the lead - scintillator sandwich type electromagnetic calorimeter (0.2cm lead and 0.5cm scintillator). The obtained results σ_E/E=11% and ΔE=76% are in a good agreement with the experiment[10].

2. The calculations for a 52x52 cm^2 module are presented to determine the effect of the lateral leakage of the shower on the calorimeter characteristics.

From the data presented in Table 3 it follows:

1. The comparison of the calorimeter module energy resolution values at 5 GeV with a consideration of Poisson fluctuations of the secondary emmision electrons number (points 6,15,19) and in their absence (points 7,16,20) shows, that Poisson fluctuations make the main contribution into the energy resolution, deteriorating it by a factor of 3. At 26 GeV the relative contribution from the Poisson fluctuations is less, but still remains decisive (points 23 and 24).

2. It follows from the points 1÷5 of the table 3, that the absorber plates thickness increase (with unchanged total calorimeter length in the units of X_0) does not noticeably affect the resolution, i.e. a growth of sampling fluctuations is compensated by a decrease of Poisson fluctuations due to a less number of layers. However, the value of the signal decreases.

3. Two values of the parameter w are used: 0.025 and 0.05. The resolution improves with a growth of w (points 1 and 6, 2 and 19), what means, that the value of w should be determined more accurately.

4. The results are dependent most noticeably on the parameter k_{mult}, which was varied from 0.9 to 1.165. The points 6,8,9 and 23,25÷32 of the table show, that with a k_{mult} deviation from one the resolution is worsening essentially, with the value of the signal growing sharply when k_{mult} increases. In addition, the comparison

of the charged longitudinal distributions of the showers, relevant to k_{mult}=1 and k_{mult}=1.13 (figs. 10 and 11, respectively), shows that with an increase of k_{mult} the charged longitudinal profile of the shower is distorted essentially. This results in the energy nonlinearity of the calorimeter response (coloumn 7 of points 17,30, compare with the points 15,23) and in distortion of the generally accepted dependence σ_E/E. Indeed, the relative energy resolution values for 5 and 26 GeV, recalculated to 1 GeV according to the usual dependence $\sigma_E/E \sim 1/\sqrt{E}$, are sharply different (coloumn 6 of the specified points). Hence, the value of k_{mult} should be close to unity.

5. The energy resolution of the calorimeter at 5 GeV for 1.5 mm thick absorber plates is 33.5% (w=0.05) and 46.5% (w=0.025) (points 1 and 6, respectively). The resolution is somewhat higher for 3 mm thick absorber plates, 31.3% and 41.8% (points 2 and 19, respectively). The last version is more preferable, because it makes the design of the calorimeter more simplified. The same situation is for 26 GeV.

6. The depth segmentation of the calorimeter allows one to decrease essentially the contribution from Poisson fluctuations into the energy resolution (points 10÷13,21). For example, segmentation just into 4 parts makes it possible to attain the resolution close to the maximum one without Poisson fluctuations. With the segmentation according to the point 13 and charge collection in the sections, as specified in column 5, the resolution is 24.9%, which is close to the maximum one, 15.2% (see point 7). In addition, in the case of segmentation, even for k_{mult}=1.165 the calorimeter is linear in energy, its resolution is sufficiently high (points 33,18) and much weaker dependent on k_{mult} (cf. points 13,14 and 6,9) with relatively small weakening of the dependence on parameter w (cf. points 2,19 and 21,22).

7. The muon detection efficiency is strongly dependent on k_{mult}. It varies from 30% (k_{mult}=1) upto 80% (k_{mult}=1.165).

Figure 12 compares the calculated dependence of σ_E/E on k_{mult} with the experimental data, obtained in this work. It is seen, that the calculated and experimental measurements of the energy resolution value differ essentially and this cannot be explained by the uncertainty in the value of w (points 30,34). From our point of view, possible reason for this difference may be the flights of secondary electrons through the absorber layers without collisions. This changes the character of the distribution for the number of secondary electrons, obtained in the calculations, by decrease its dispersion. This assumption needs to be checked carefully, because it can lead to an essential improvement of the energy resolution of similar calorimeters and decreases the time of flight of secondary emission electrons. The triangle in this figure denotes the Monte Carlo result for segmented into 4 parts calorimeter at

5 GeV (point 13), recalculated to 26 GeV. The result presented characterizes the maximum attainable resolution for the chosen structure.

The authors would like to express their deep gratitude to Yu.D. Prokoshkin for the support of the present work and fruitful discussions, to A.M.Gorin, V.I.Kireev, Yu.P.Petukhov, V.I.Spiryakin and V.P.Sugonyaev and also to the teams of MIS ITEP and PROZA for their assistance in measurements.

Figure Captions

Fig.1 The schematic view of the secondary emission flight type calorimeter: 1–shutter dynodes from a photoelectron multiplier, 2–glass rod, 3–glass bushing, 4–brass frame, 5–lead strip of the absorber, 6–metal grid, 7–secondary electron multiplier, 8–amplifier.

Fig.2 The scheme of studying of secondary emission flight type calorimeter.

Fig.3 The scheme of measurment of the layer multiplication coefficient k_{mult} dependence upon the intercascade voltage U_c.

Fig.4 The multiplication coefficient k_{mult} of the layer versus the intercascade voltage U_c.

Fig.5 The amplitude spectra from the ultraviolet laser: the right-hand spectrum—the laser ray is not attenuated, the left-hand spectrum—attenuated by crossing of 18 mm Plexiglas.

Fig.6 The dependence of $(2\tau/\mathrm{A})^2$ upon $1/\mathrm{A}$.

Fig.7 The experimentally measured amplitude spectra for 26 GeV electrons for different values of the intercascade voltage U_c (k_{mult}).

Fig.8 The experimentally measured amplitude spectrum of muons.

Fig.9 The basic calculated characteristics of the electromagnetic shower in secondary emission flight type calorimeter (SEFCAL): (a) the spectrum of the total energy deposition in the calorimeter in % of the energy causing the particle shower; (b) the longitudinal profile of electromagnetic shower—the relative energy deposition vs the number of layers; (c) the transverse profile of the shower—the relative energy deposition vs the number of longitudinal strips in a layer, summed over the whole depth; (d) the measured charged spectrum N_e in absence of Poisson fluctuations of the number of secondary emission electrons.

Fig.10 The charged longitudinal distribution of shower—the average numbers of secondary emission electrons vs the number of layers (left) and the charged spectra (right) for different values of the parameters k_{mult} and w at 5 GeV/c.

Fig.11 The charged longitudinal distribution of shower—the number of emission electrons vs the number of layers (left) and the charged spectra (right) for different values of the parameters k_{mult} and w at 26 GeV/c.

Fig.12 The comparison of the calculated dependence of σ_E/E upon k_{mult} with the experimental data.

References

[1] Letters of Intent to the SSC Laboratory from EMPACT, L*, TEXAS and SD Collaborations, 1990.

[2] R.N.Krasnokutsky et al. Cable Connections for Detector and Preamplifier, Eliminating Radiation Damage of Electronics. Preprint IHEP 91-48, Protvino 1991.

[3] M.Kobayashi et al., Nucl. Instr. Meth. A302(1991)443; G.I.Britvich et al. Nucl. Instr. Meth. A308(1991)509; M.Kobayashi and M.Ishii, Nucl. Instr. Meth. B61(1991)491.

[4] A.A.Derevshchikov et al., On Possibility to Make a New Type of Calorimeter: Radiation Resistant and Fast. IHEP preprint 90-99, Protvino, 1990.

[5] G.S.Bitsadze, A.M.Medvedkov and V.I.Rykalin, On the Possibility of Design of Secondary Emission Flight Type Calorimeter, III WORKSHOP "PHYSICS AT UNK", 25-28 September 1990, Protvino, USSR (in Press).

[6] V.Agoritsas, Secondary Emission Chambers for Monitoring the CPS Ejected Beams, SYMPOSIUM ON BEAM INTENSITY MEASUREMENT, Daresbury,22-26 April 1968, p.117.

[7] F.Binon et al., Data Acquisition System for the GAMS-2000 Spectrometer, Preprint IHEP 88-179, Serpukhov 1988.

[8] R.Brun et al., Preprint CERN - DD/EE/84-1, 1987.

[9] H.L.Seifert et al., Increased Secondary Electron Yield from Thin CsI Coatings, LA UR -90-713, Los-Alamos, 1990.

[10] A.N.Vasiliev et al. Preprint IHEP 82-62, Serpukhov, 1982.

Table 1: Requirements on forward calorimeters in SSC and LHC projects

Projects	Calorimeter type	Energy resolution	Magnetic field	Possible active media
SDC	hadron	$<1.0/\sqrt{E}\otimes 0.05$	absent	warm liquid, liq.scint. fibres, high pres.gases
L*	hadron el.magnetic	$54\%/\sqrt{E}+2\%$ $17\%/\sqrt{E}+1\%$	absent	warm liquid TMS
EMPACT	hadron	$0.5/\sqrt{E}+0.02$	absent	liq.argon, SPACAL
LHC+	hadron	$\sqrt{\frac{(0.65)^2}{\sqrt{E}}+\frac{(0.1)^2}{E^2}}$	absent	Xe/CH_4

$\otimes$ - term added quadratically
+ - C.W.Fabjan private communication

Table 2: Possible candidates for forward calorimeter

Calorimeter type	Maximum yearly dose, Mrad	Element, determining radiation hardness	Information sourse
ionization, warm liquids, cold (noble) liquids, compressed gases	≤ 10	semiconductor elements of electronics	LHC WORKSHOP Oct.1990 Aachen
single cristal, scintillation and Cerencov	≥ 100 for number of materials	single crystal, scintillator or radiator, photocathode	/3/
based on secondary emission: MCP, metall emitters	? ≥ 100	MCP, emitters	/4/ present work

Table 3: Results on calculation of secondary emission flight type calorimeter

N	E GeV	Emis. prob.	Pb-thick (cm)	Segmentation	σE/E (%)	N_e	ΔE (%)	S (cm^2)	k_{mult}
1	2	3	4	5	6	7	8	9	10
1	5	0,05	0,15		33,5	1266	93	52x52	1
2	5	0,05	0,3		31,3	736	94	52x52	1
3	5	0,05	0,5		31,2	510	94	52x52	1
4	5	0,05	0,8		31,3	433	96	52x52	1
5	5	0,05	1,2		32,2	370	95	52x52	1
6	5	0,025	0,15		46,5	648	93	52x52	1
7	(No Poisson fluctuations)				15,2	635	93	52x52	1
8	5	0,025	0,15		51,3	1326	92	52x52	1,03
9	5	0,025	0,15		98,8	73515	92	52x52	1,165
10	5	0,025	0,15	25,25	34,5	638	92	52x52	1
11	5	0,025	0,15	25,25	37,6	637	93	52x52	1
12	5	0,025	0,15	24,26	29,5	633	93	52x52	1
13	5	0,025	0,15	18,10,10,12	24,9	635	93	52x52	1
14	5	0,025	0,15	18,10,10,12	29,2	1427	93	52x52	1,165
15	5	0,025	0,15		55,4	467	78	10x10	1
16	(No Poisson fluctuations)				15,4	462	78	10x10	1
17	5	0,025	0,15		91,8	20057	78	10x10	1,13
18	5	0,025	0,15	18,10,10,12	31,4	1020	78	10x10	1,165
19	5	0,025	0,3		41,8	361	90	52x52	1
20	(No Poisson fluctuations)				19,2	359	90	52x52	1
21	5	0,025	0,3	10,9,6	32,3	359	90	52x52	1
22	5	0,05	0,3	10,9,6	25,0	717	90	52x52	1
23	26	0,025	0,15		57,9	2387	76	10x10	1
24	(No Poisson fluctuations)				33,5	2382	76	10x10	1
25	26	0,025	0,15		128,1	411	76	10x10	0,90
26	26	0,025	0,15		76,1	890	76	10x10	0,95
27	26	0,025	0,15		84,3	4768	76	10x10	1,03
28	26	0,025	0,15		117,2	10140	76	10x10	1,06
29	26	0,025	0,15		163,1	29853	76	10x10	1,10
30	26	0,025	0,15		188,5	69410	76	10x10	1,13
31	26	0,025	0,15		201,4	106900	76	10x10	1,145
32	26	0,025	0,15		220,4	191339	76	10x10	1,165
33	26	0,025	0,15	18,10,10,12	35,7	5176	76	10x10	1,165
34	26	0,05	0,15		185,2	138091	76	10x10	1,13

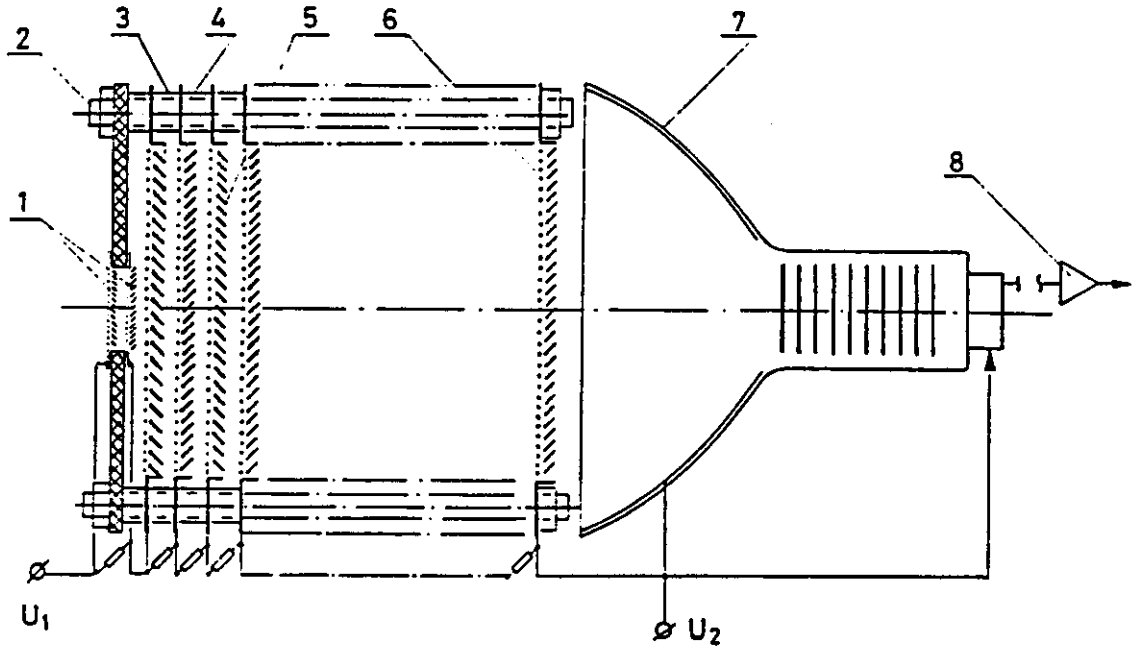

Fig. 1.

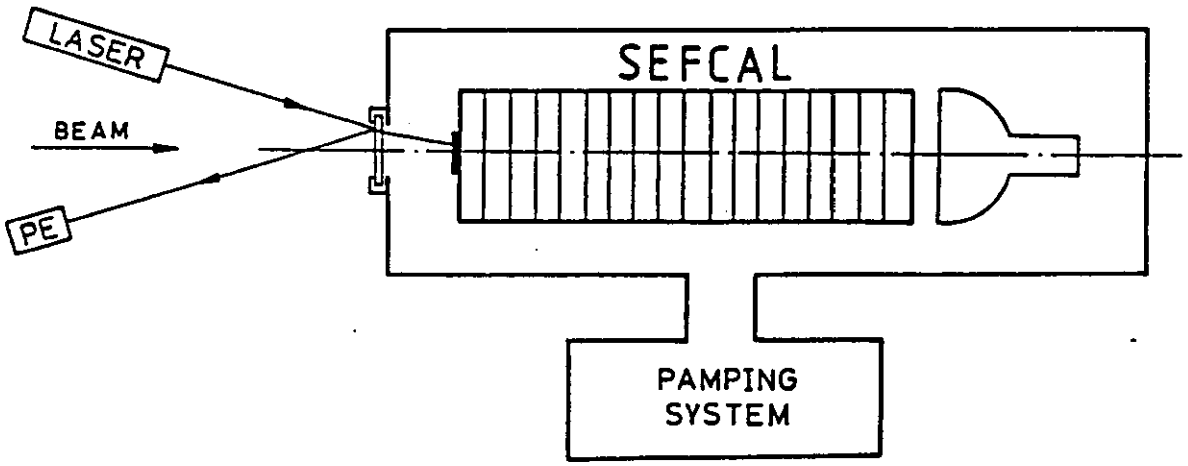

Fig. 2.

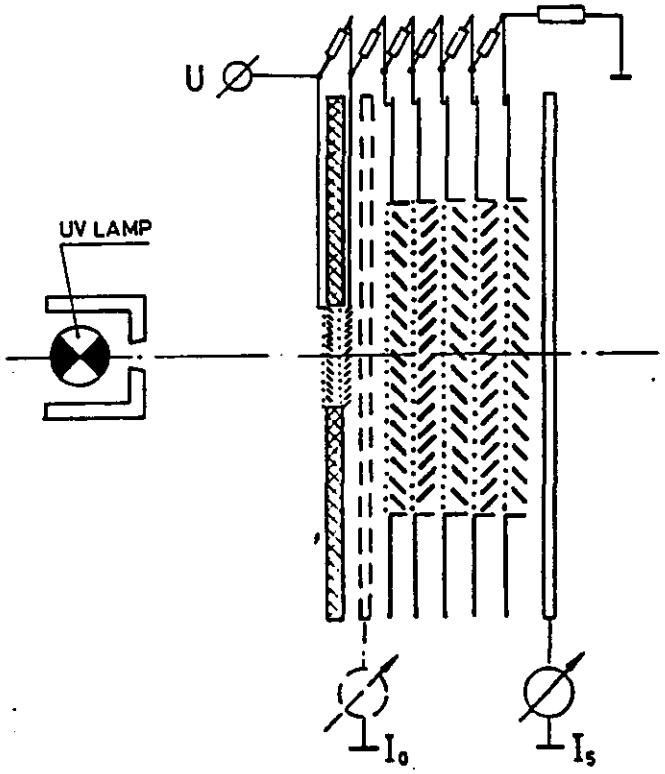
U
UV LAMP
I_0
I_s

Fig. 3.

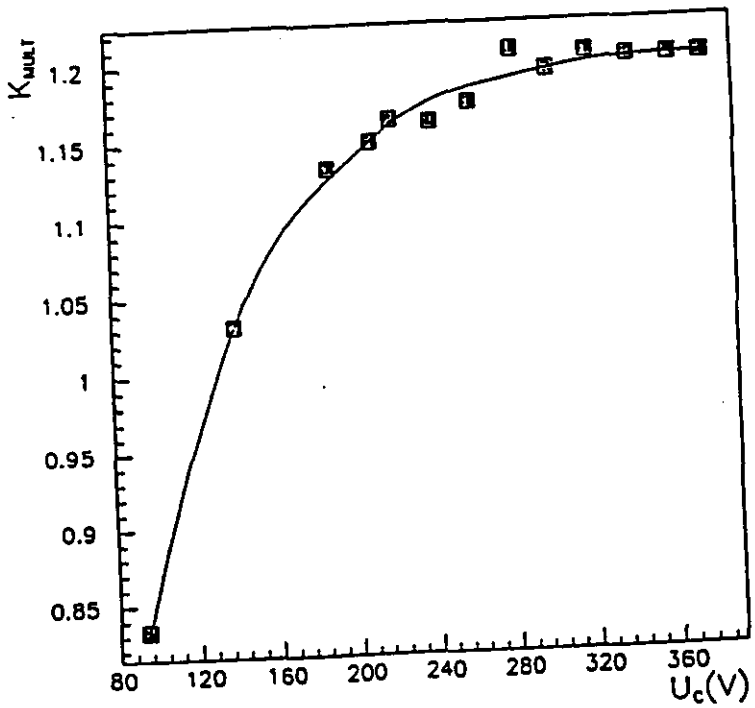
K_{MULT}
1.2
1.15
1.1
1.05
1
0.95
0.9
0.85
80
120
160
200
240
280
320
360
U_c(V)

Fig. 4.

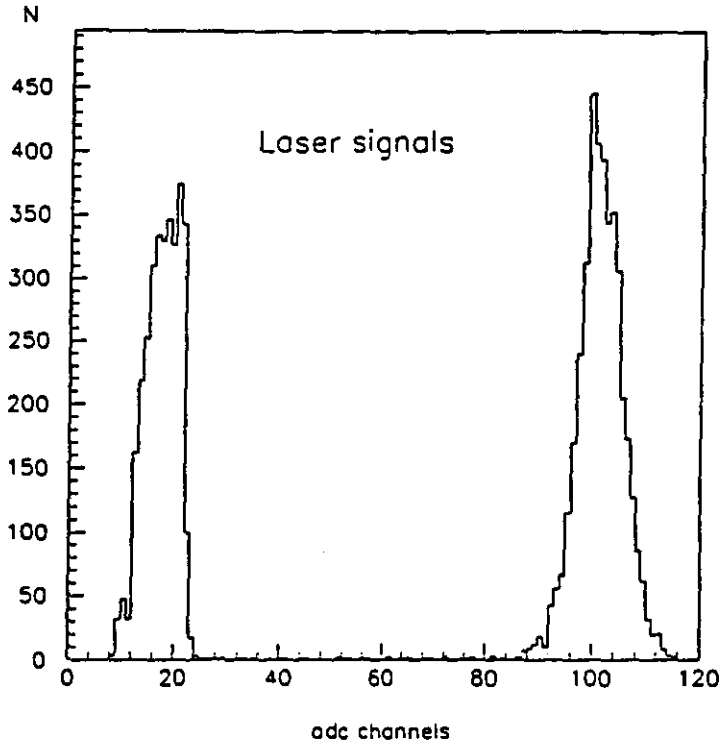

Fig. 5.

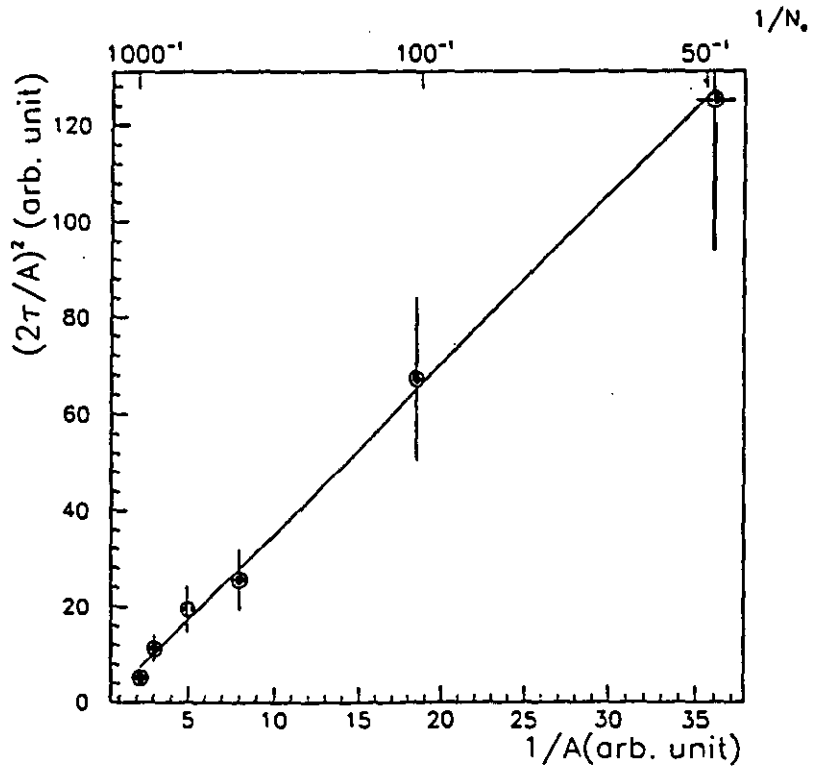

Fig. 6.

e 26 GeV/c

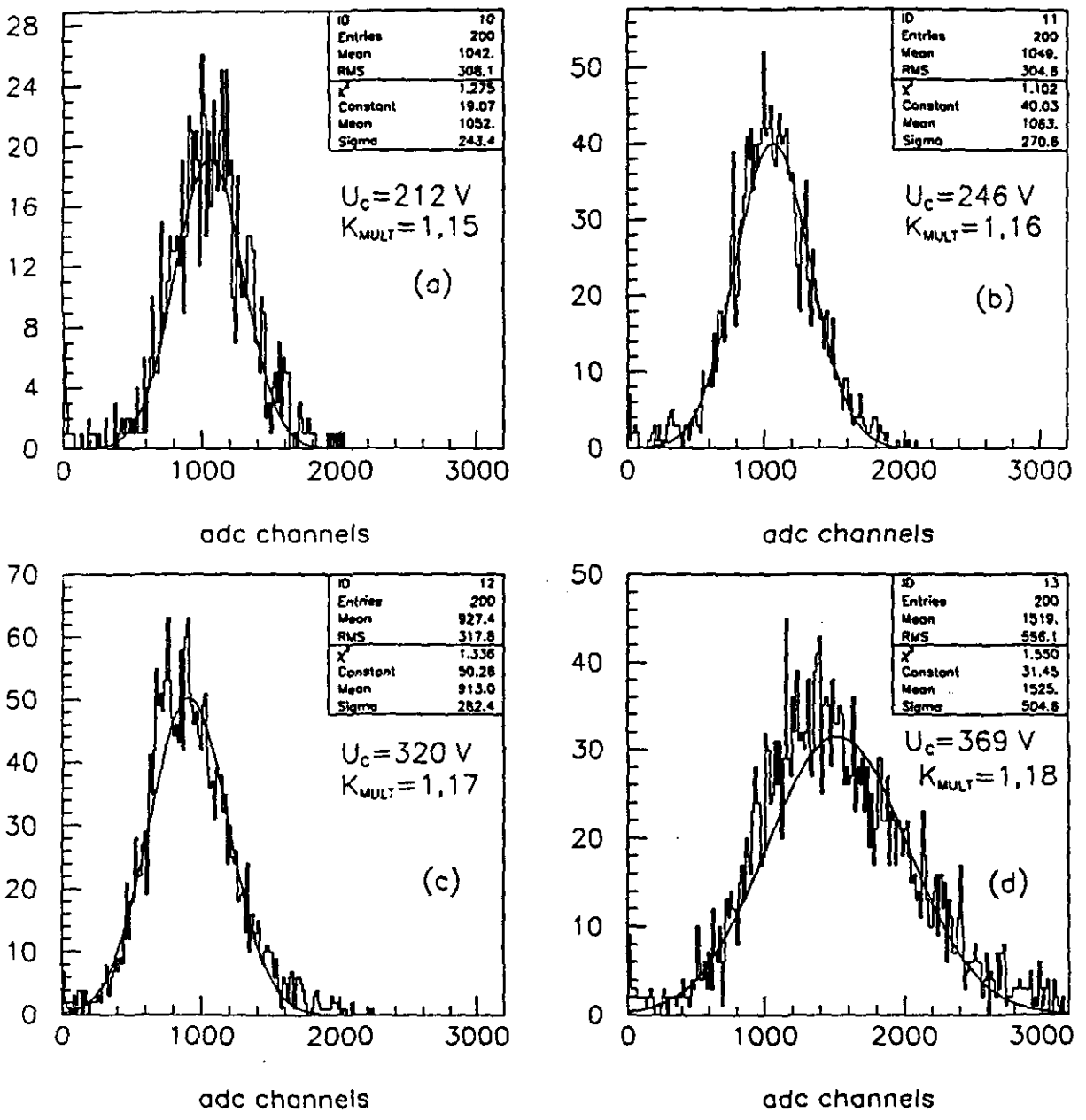

Fig. 7.

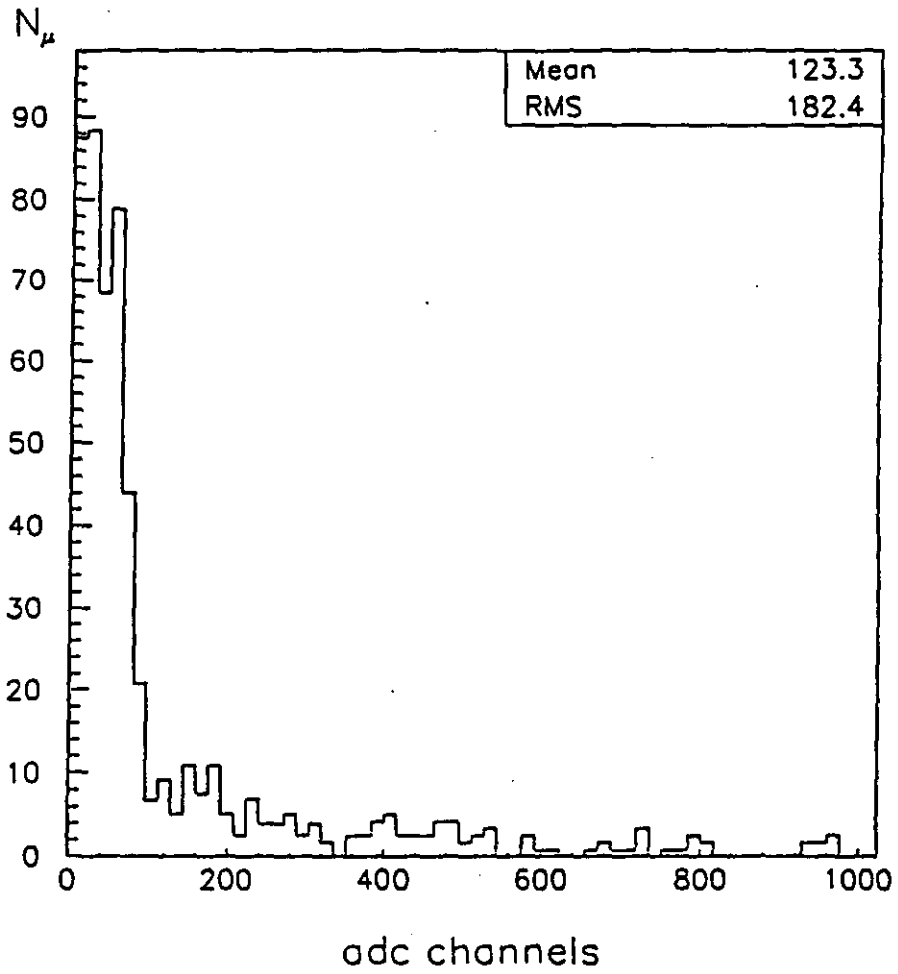
N_μ
Mean 123.3
RMS 182.4
90
80
70
60
50
40
30
20
10
0
0
200
400
600
800
1000
adc channels

Fig. 8.

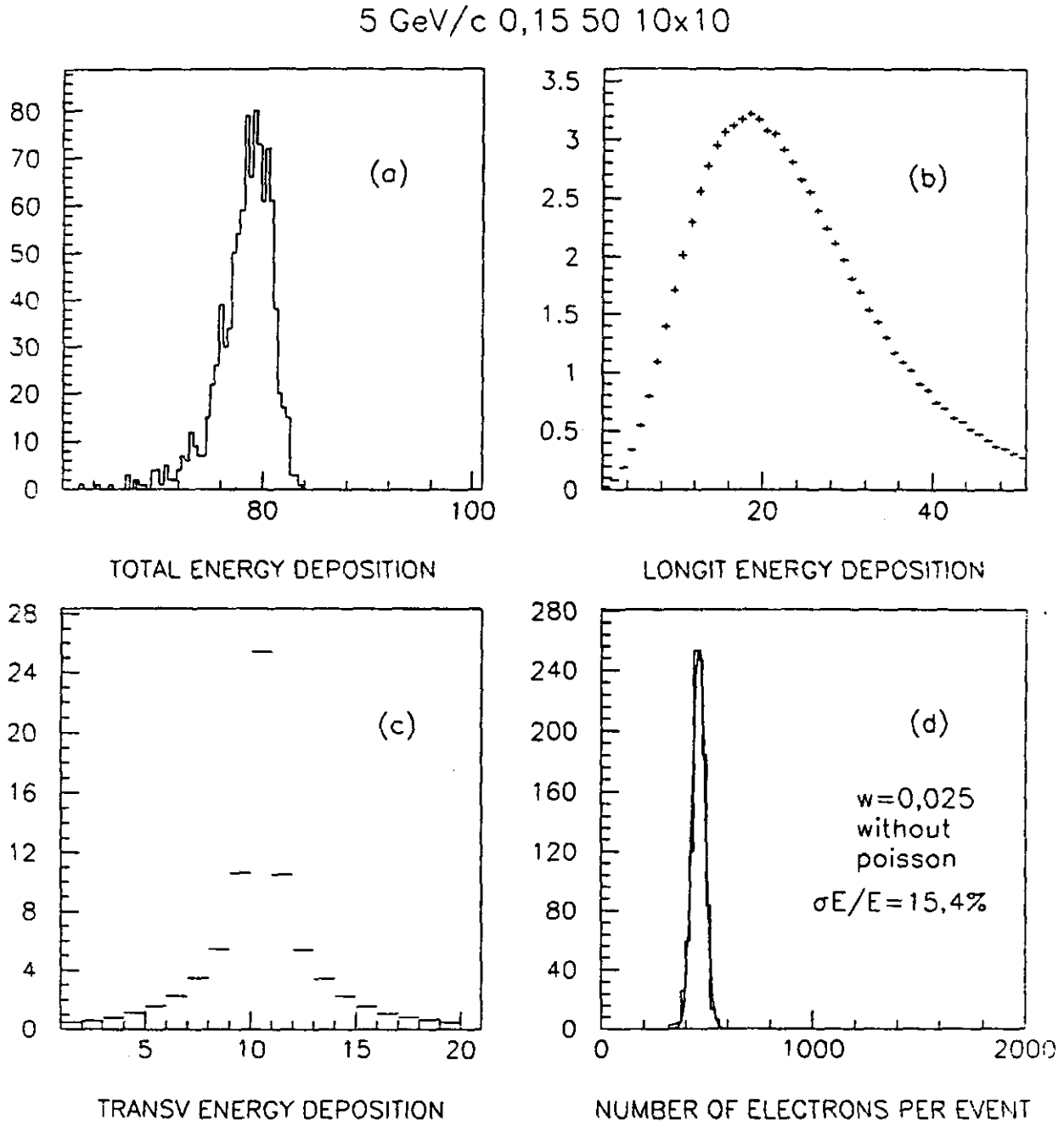
5 GeV/c 0,15 50 10x10
(a)
(b)
TOTAL ENERGY DEPOSITION
LONGIT ENERGY DEPOSITION
(c)
(d)
w=0,025
without
poisson
σE/E=15,4%
TRANSV ENERGY DEPOSITION
NUMBER OF ELECTRONS PER EVENT

Fig. 9.

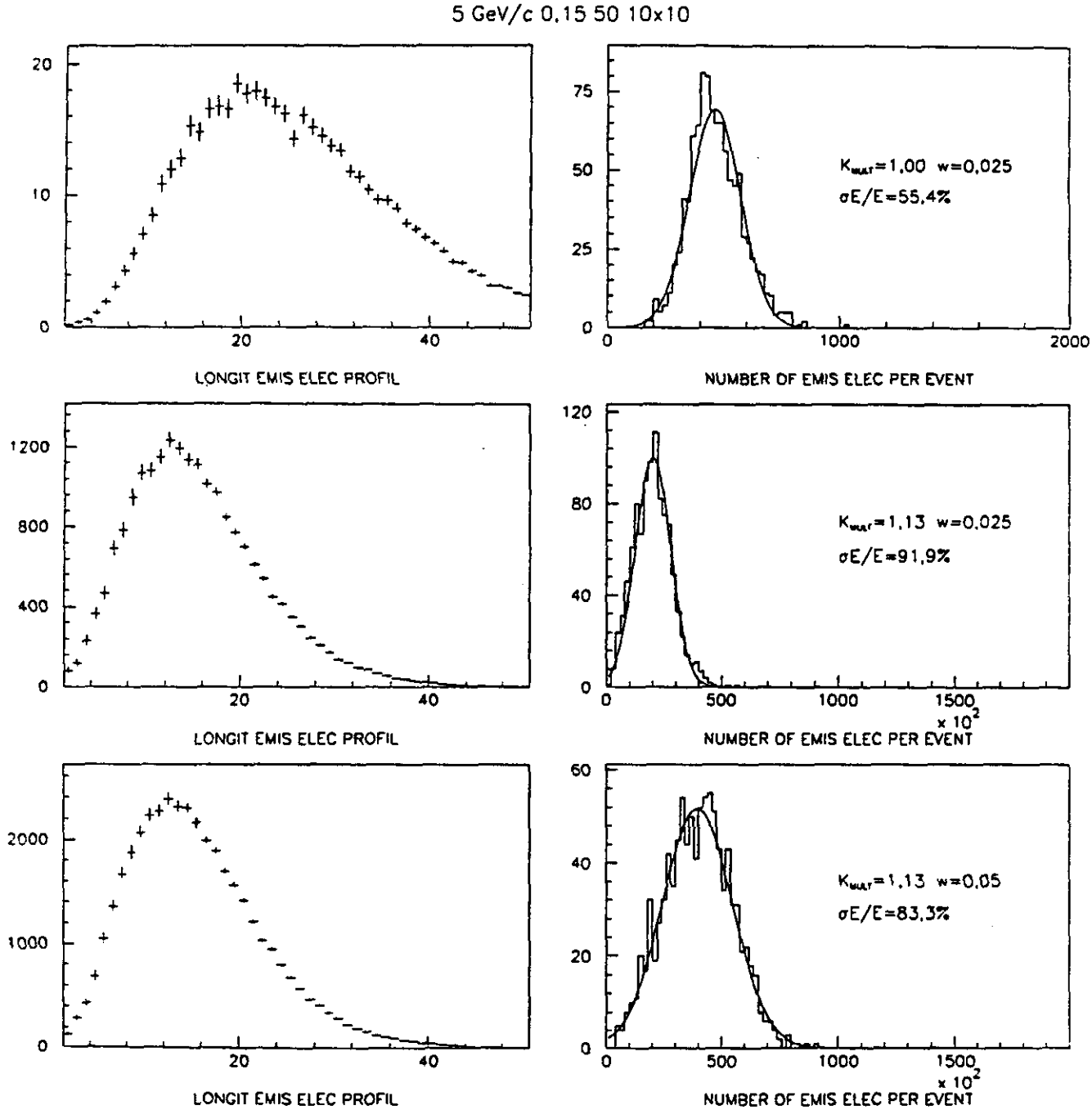
5 GeV/c 0,15 50 10x10
LONGIT EMIS ELEC PROFIL
NUMBER OF EMIS ELEC PER EVENT
K=1,00 w=0,025
σE/E=55,4%
LONGIT EMIS ELEC PROFIL
NUMBER OF EMIS ELEC PER EVENT
K=1,13 w=0,025
σE/E=91,9%
LONGIT EMIS ELEC PROFIL
NUMBER OF EMIS ELEC PER EVENT
K=1,13 w=0,05
σE/E=83,3%

Fig. 10.

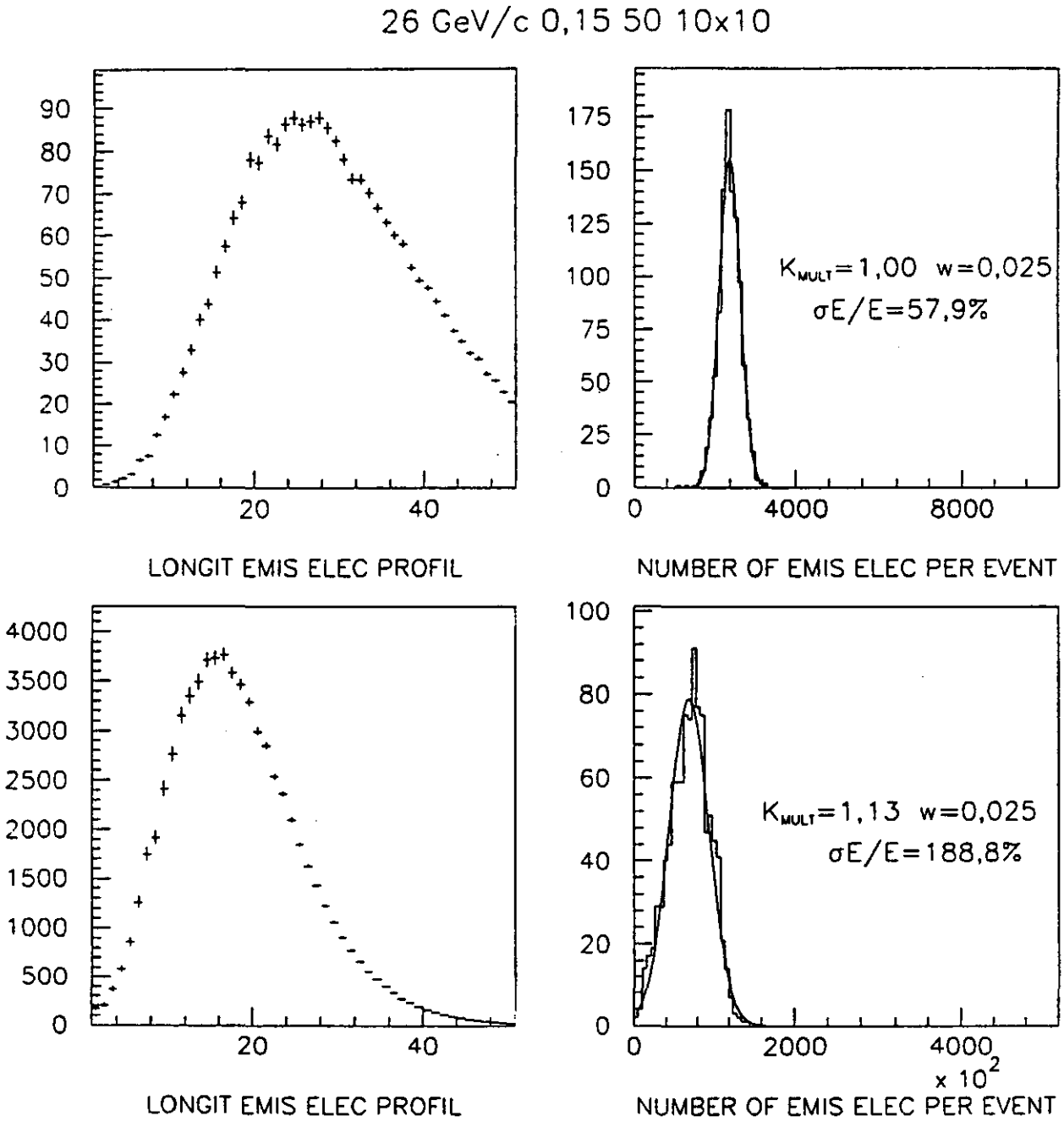
26 GeV/c 0,15 50 10x10
LONGIT EMIS ELEC PROFIL
NUMBER OF EMIS ELEC PER EVENT
K_{MULT}=1,00 w=0,025
σE/E=57,9%
LONGIT EMIS ELEC PROFIL
NUMBER OF EMIS ELEC PER EVENT
K_{MULT}=1,13 w=0,025
σE/E=188,8%
x 10^2

Fig. 11.

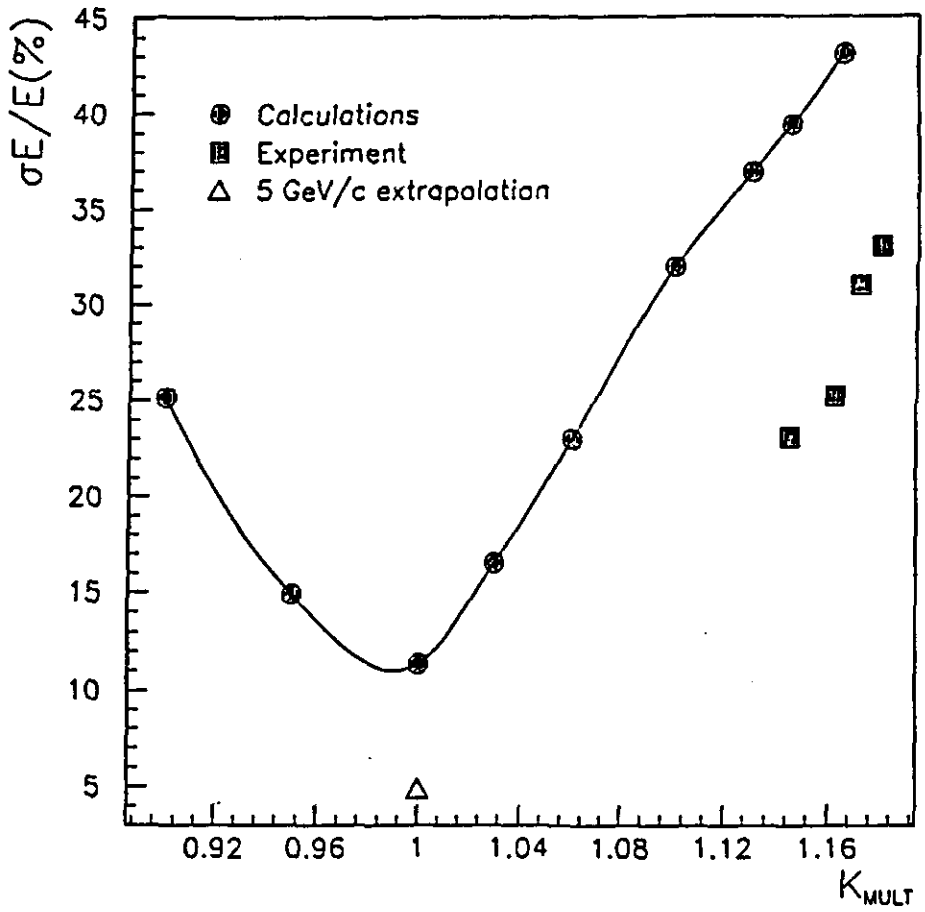
σE/E(%)
45
40
35
30
25
20
15
10
5
Calculations
Experiment
5 GeV/c extrapolation
0.92
0.96
1
1.04
1.08
1.12
1.16
K_MULT

Fig. 12.